

Conformal-invariance of 2D quantum turbulence in an exciton-polariton fluid of light

R. Panico,¹ A. S. Lanotte,^{1,2} D. Trypogeorgos,¹ G. Gigli,^{1,3} M. De Giorgi,¹ D. Sanvitto,¹ and D. Ballarini¹

¹*CNR NANOTEC, Institute of Nanotechnology, Via Monteroni, 73100 Lecce, Italy*

²*INFN, Sez. Lecce, 73100 Lecce, Italy*

³*Dipartimento di Matematica e Fisica E. De Giorgi, Università del Salento, Campus Ecotekne, via Monteroni, Lecce 73100, Italy*

(*Electronic mail: dario.ballarini@nanotec.cnr.it)

(Dated: 3 July 2023)

The similarities of quantum turbulence with classical hydrodynamics allow quantum fluids to provide essential models of their classical analogue, paving the way for fundamental advances in physics and technology. Recently, experiments on 2D quantum turbulence observed the clustering of same-sign vortices in strong analogy with the inverse energy cascade of classical fluids. However, self-similarity of the turbulent flow, a fundamental concept in the study of classical turbulence, has so far remained largely unexplored in quantum systems. Here, thanks to the unique features of exciton-polaritons, we measure the scale invariance of velocity circulations and show that the cascade process follows the universal scaling of critical phenomena in 2D. We demonstrate this behaviour from the statistical analysis of the experimentally measured incompressible velocity field and the microscopic imaging of the quantum fluid. These results can find wide application in both quantum and classical 2D turbulence.

I. INTRODUCTION

Turbulent dynamics in classical fluids has been first identified by A. N. Kolmogorov with the presence of a self-similar energy cascade. Self-similarity, or scale invariance, refers to the statistically identical behaviour of the velocity fluctuations after scale transformations. In three dimensions (3D), the existence of non-zero energy dissipation even in the limit of zero viscosity implies a direct energy cascade from a large injection scale towards smaller spatial scales¹. In 2D, the picture is different due to the existence of an additional integral of motion given by enstrophy. Since energy and enstrophy can not cascade in the same direction², in 2D the kinetic energy flows from the injection scale towards larger structures (inverse energy cascade), while enstrophy undergoes a direct cascade to smaller scales^{3,4}.

A subtler consequence of the direction of the cascade concerns the presence of intermittency, that is the deviation from self-similarity. Indeed, direct turbulent cascades are generally not scale invariant⁵, in connection with the non-gaussian nature of the small-scales viscous processes. This is the case for 3D turbulence, where most of the kinetic energy is dissipated within spatially localised structures. This intermittent statistics of energy dissipation breaks the original Kolmogorov assumption of self-similarity of the cascade process^{6,7}. The 2D energy cascade in classical turbulence is fundamentally different: the presence of intermittency in the inverse transfer process has been ruled out^{4,8,9}, intuitively because the energy fluxes are directed towards larger structures where extreme events due to energy dissipation play no role. Hence velocity fluctuations are scale-invariant in the inverse energy cascade.

Quantum turbulence, differently from its classical counterpart, is intrinsically singular, since its basic constituents are discrete, quantised vortices of unitary topological charge. Quantum vortices resemble the point vortex model proposed by L. Onsager, who described the final stage of the inverse cascade as an equilibrium state in a negative temperature

regime^{10,11}. The experimental investigation of quantum turbulence, which began with superfluid helium^{12,13}, has made great progress with the realisation of Bose-Einstein condensates (BEC) of ultracold atoms^{14–17}. One of the main reasons why BECs are important for the study of quantum turbulence is the possibility of visualising individual vortices and describing their dynamics on a microscopic level¹⁸. On the other hand, an open question is how to bridge the gap between the discrete picture of quantum vortices and the self-similar nature of classical inverse energy cascade^{19–21}. In particular, we wonder whether the self-similar spatial correlations may nonetheless emerge in the velocity field of a quantum fluid, and which are the roots of this evidence in the system dynamics.

For this purpose, we use an optical system, exciton-polaritons in semiconductor microcavities. These hybrid light-matter quasiparticles have been shown in the last decades to behave like a quantum fluid of light, manifesting out-of-equilibrium Bose-Einstein condensation and superfluidity^{22–25}. We have recently shown that, under suitable initial conditions, it is possible to induce an inverse cascade of incompressible kinetic energy in 2D polariton quantum fluids²⁶. Crucially, these systems allow the measurement of the spatial distribution of the velocity field with high accuracy, enabling a robust statistical analysis^{27,28}.

Here, thanks to the direct measurement of the phase of the polariton field, we are able to extract the statistics of the incompressible velocity in the inverse energy cascade of a quantum fluid. While the singular nature of quantised vortices manifests itself in the large tails of velocity increment distribution, the velocity circulations (or vorticity fluxes) show remarkable scale invariant properties. Moreover, we find that a coarse graining of the vorticity field allows the identification of macro-regions of aligned vortex-antivortex dipoles that are responsible for the appearance of long-range order in the system. We show that the statistical distribution and fractal dimension of the regions with correlated vorticity follow the

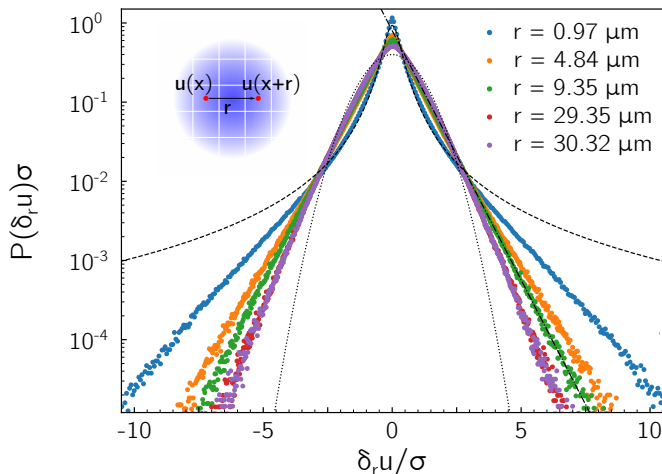


FIG. 1. a) Probability density functions (PDF) of the longitudinal velocity increments $\delta_r u \equiv \frac{\mathbf{r}}{r} \cdot [\mathbf{u}(\mathbf{x} + \mathbf{r}) - \mathbf{u}(\mathbf{x})]$ at scale r , normalised to their standard deviation $\sigma = \langle (\delta_r u)^2 \rangle^{1/2}$. For sub-healing length scales, $r < \xi = 2.3 \mu\text{m}$, the PDF follows a Cauchy-Lorentz distribution (dashed line), while at increasing r it slowly approaches a Gaussian (dotted line). For every scale, the tails of the distribution are exponential (dashed-dotted line). The lack of a self-similar rescaling of the PDFs is an indication of intermittency.

critical behaviour predicted near phase transition in percolation theory. This analysis goes beyond the classification of first-neighbour vortices and opens to the investigation of spatial symmetries in 2D quantum turbulence.

II. MAIN RESULTS

We use the same experimental configuration described in a previous work²⁶ to induce vortex clustering and a transient regime of inverse kinetic energy cascade after the expansion of a polariton quantum fluid in a confining potential. The typical number of vortices is $N > 80$, with intervortex distances $\approx 2\xi$ and diameter of the confining ring potential $> 50\xi$. For our analysis, we consider the incompressible velocity field $\mathbf{u}(\mathbf{x}, t)$ of the 2D polariton fluid described by the wave-function $\psi(\mathbf{x}, t) = \sqrt{\rho(\mathbf{x}, t)}e^{-i\theta(\mathbf{x}, t)}$, in the time interval corresponding to the inverse energy cascade. The total velocity field is given by the gradient of the phase θ as

$$\mathbf{v}(\mathbf{x}, t) = \frac{\hbar}{m} \nabla \theta(\mathbf{x}, t), \quad (1)$$

where m is the polariton mass. The phase of the polariton fluid is obtained from time-resolved interferometric measurements of the photons emitted by the microcavity, while the incompressible component $\mathbf{u}(\mathbf{x}, t)$ of the velocity field is determined at any point in space by applying the Helmholtz decomposition to the density weighted velocity $\sqrt{\rho}\mathbf{v}$ ²⁶. We use about 125K pixels per image with a spatial resolution $s \sim 0.14\xi$, being $\xi = 2.3 \mu\text{m}$ the estimated healing length of the quantum fluid. To improve statistical accuracy, we average over larger time intervals (always within the inverse energy cascade window), and over few realisations of the experiment in different

locations of the sample. In the following, we show the statistics over a total number of pixels $\approx 2 \cdot 10^7$ (accounting for the longitudinal increments along both x and y axis).

In Fig. 1, the probability density function (PDF) of the longitudinal velocity increments $\delta_r u \equiv \frac{\mathbf{r}}{r} \cdot [\mathbf{u}(\mathbf{x} + \mathbf{r}) - \mathbf{u}(\mathbf{x})]$, where the velocity \mathbf{u} and the separation \mathbf{r} vectors are taken in the same direction, are shown for increasing spatial scale $r = |\mathbf{r}|$, from $r \simeq 0.4\xi$ to $r \simeq 14\xi$. At very small scales, the velocity increment PDF follows a Cauchy distribution, while it gradually approaches a Gaussian distribution as the scale increases²⁹. The presence of exponential tails in the distribution is clearly visible for every distance, indicating a finite probability of large $|\delta_r u|$ events. This follows directly from the presence of quantised vortices, where velocity increments manifest their singular behaviour²⁹. This reflects as well in the lack of self-similarity of the PDFs when rescaled to their standard deviations as in Fig. 1 – self-similarity would entail a collapse of the PDFs onto a single curve, as observed in the classical case⁹. This intermittent behaviour is intrinsic to the quantum system and can be related to the fact that energy is injected spontaneously through the nucleation of vortex dipoles at the healing length scale³⁰.

While the distribution of the velocity increments is not a good observable to look for scale-invariant properties in a quantum fluid, moments of velocity circulation has recently been proposed as a more fundamental and unifying quantity^{31–33}. Velocity circulation is defined as

$$\Gamma_R(\mathbf{x}) = \oint_{C_R} \mathbf{u}(\mathbf{x}') \cdot d\mathbf{x}', \quad (2)$$

where C_R is a square loop with opposite corners $(x - R/2, y - R/2)$ and $(x + R/2, y + R/2)$, while \mathbf{u} is the incompressible velocity. In Fig. 2, we show the PDFs of the velocity circulation, measured on closed loops of size R . The most striking feature is that scale invariance now holds: contrary to the case of velocity increments, the PDF of the velocity circulation on loops of different size rescale with their standard deviation and collapse on a single (exponential) distribution. Incidentally, we remark that at difference with the locality regime of classical inverse cascade, the scaling behaviours of velocity and vorticity cannot be directly linked in a quantum system.

Self-similarity is a strong feature that suggests the quest for other global symmetries. Numerical results on classical 2D turbulence have shown that lines of zero-vorticity, i.e. the boundaries of high vorticity regions, are stochastic Schramm-Loewner evolution (SLE_κ) curves³⁴. The SLE curves univocally describe the conformal invariant scaling limit of the interfaces of many 2D critical models, with the parameter κ defining the universal behavior close to threshold. The same universality class was predicted for cluster boundaries of critical percolation, one of the most fundamental models of phase transition, and the isovorticity lines in the inverse energy cascade, also for weakly compressible fluids³⁵.

To explore the appearance of conformal invariant interfaces in 2D quantum turbulence, we consider a continuous field of coarse-grained vorticity $\omega = \nabla \times \mathbf{u}$ (i.e. its flux), defined at each point in space as the value of velocity circulation $\Gamma_R(\mathbf{x})$ over a square loop of size comparable to the healing length ξ .

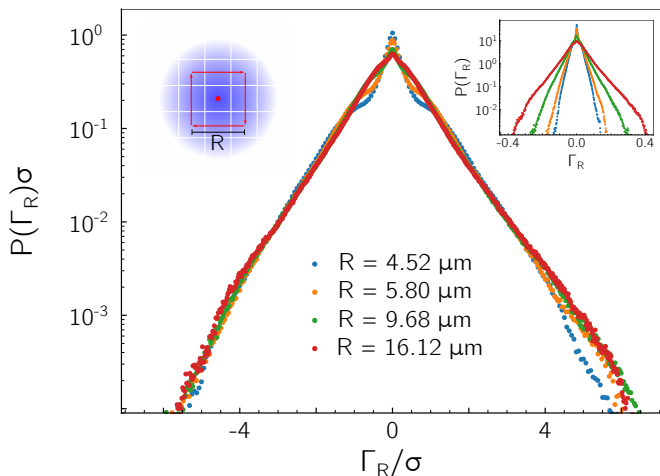


FIG. 2. PDF of the velocity circulation for loops of size R , defined as Eq.3, normalised to its standard deviation $\sigma \equiv \langle \Gamma_R^2 \rangle^{1/2}$. The inset shows the PDFs for the velocity circulations Γ_R without rescaling.

Via the Stokes' theorem, we calculate for each point $\mathbf{x} = (x, y)$ the vorticity flux through the surface S_R enclosed in the loop C_R as

$$\Gamma_R(\mathbf{x}) = \int_{S_R} (\nabla \times \mathbf{u}(\mathbf{x}')) \cdot d\mathbf{S}_R(\mathbf{x}'). \quad (3)$$

The scalar field $\Gamma_R(\mathbf{x})$ combines the information about the sign and distribution of dipoles, smoothing the singularities of quantum vortices. The 2D maps of $\Gamma_R(\mathbf{x})$ are binarized using an upper (lower) threshold to identify the areas with correlated vorticity (see methods). In Fig. 3a, we show a typical 2D map for $\Gamma_{2\xi}(\mathbf{x})$ with a threshold of 10% of its maximum value. In Fig. 3b, the region within the black circle in Fig. 3a is magnified to show the underlying organization of vortices and velocity streamlines. The regions with same sign of $\Gamma_{2\xi}(\mathbf{x})$ are indicated in red and blue, for positive and negative fluxes, respectively. Vortices and antivortices are also indicated in Fig. 3b, showing the close relation between dipole orientation and the formation of extended regions with similar vorticity. While a first neighbour classification would only count the presence of a large number of dipoles, here we identify clusters of aligned vortex dipoles forming coherent structures that extend over several healing lengths.

We focus on the statistics of the vorticity (flux) clusters and on that of their boundaries, for which percolation theory predictions have already been tested in classical turbulence^{34,35}. In Fig. 4a, we show the distribution $n(A)$ of regions with area A , identified as in Fig. 3b. The PDF decreases as a power law $n(A) \propto A^{-\alpha}$, with the same exponent α independently from the threshold used. The dashed black line scales as $\propto A^{-96/91-1}$ and characterises the cluster size distribution at the percolation threshold³⁶, showing good agreement with the experimental results above the healing length. In the absence of the energy cascade, we do not observe such clear scaling of the size distribution, as shown in the SI.

One of the central predictions for SLE curves is their fractal dimension, which is known to be $D = 1 + \kappa/8$ and, for per-

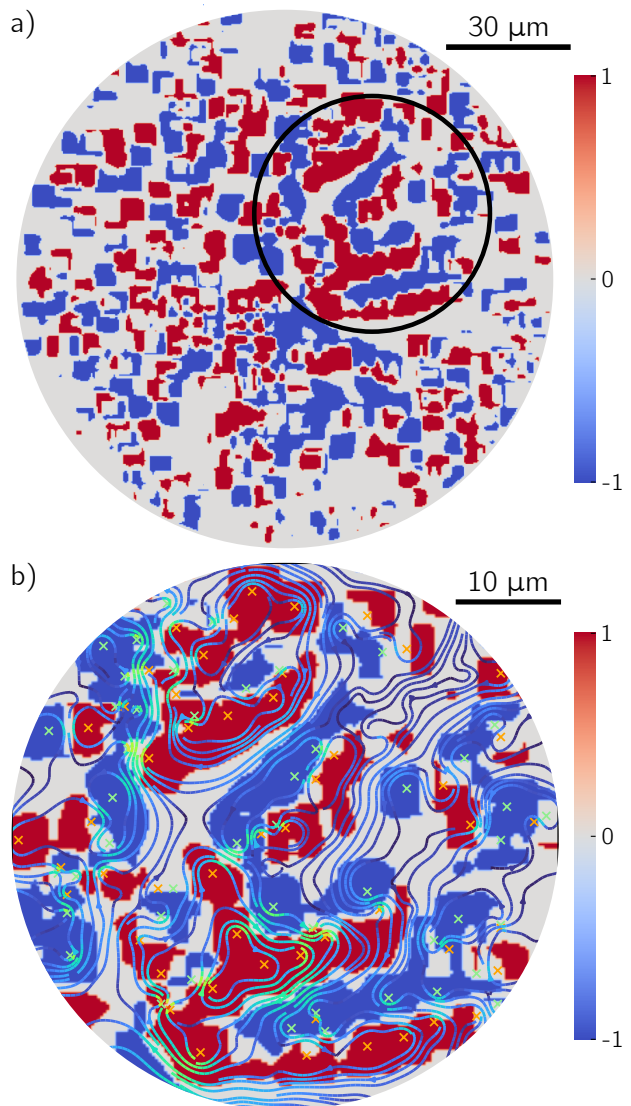


FIG. 3. a) Circulation map of a single frame obtained using Eq. 3 with $R \simeq \xi$, showing the connected areas with a circulation value above 10% of its maximum. b) Zoom of the spatial region (black circle in a), to better contrast areas of iso-vorticity flux with respect to the velocity field streamlines; the positions of the vortices (orange) and antivortices (green) are also reported. The overlap between closed velocity lines and the areas we identified is considerable and directly related to specific orientation of the dipoles.

colation, $\kappa = 6$ and $D = 7/4$. In Fig. 4b, we plot the perimeter $\mathcal{P}(A)$ versus the square root of the intrinsic area A of the connected regions. A clear scaling $\mathcal{P}(A) \propto (\sqrt{A})^D$ appears, with the exponent D , indicating the fractal dimension, which is $D > 1$. The black line in Fig. 4b is the SLE prediction for percolation, $D = 7/4$, which shows a good agreement with the experimental results above the healing length. In the absence of the inverse energy cascade, the perimeter-area scaling is limited by the smaller spatial extension of the isovorticity regions (see SI), which have maximum size of $\approx 2.5\xi$ as compared to more than 10ξ in Fig. 4b.

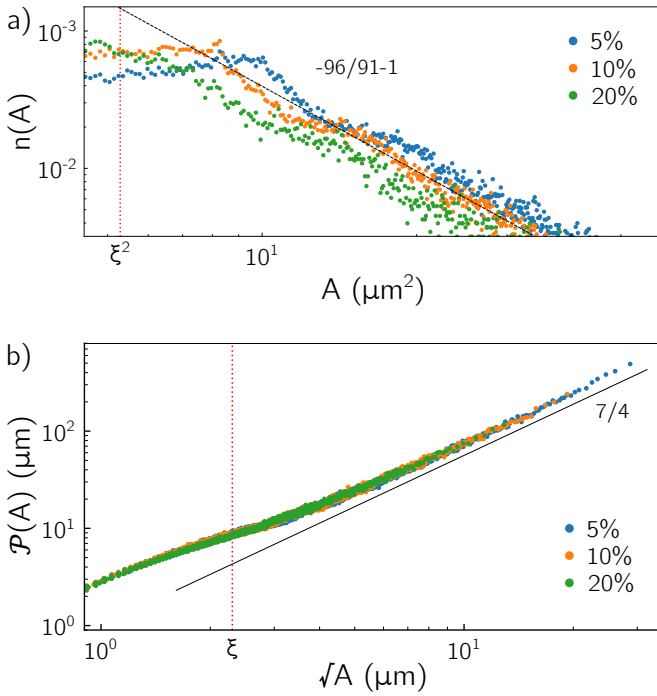


FIG. 4. a) Distribution of the extension of the connected areas of iso-vorticity flux; threshold values (5%, 10%, 20%) are referred to the maximum value. The distribution scales with the exponent $\alpha \simeq 96/91 + 1 \simeq 2.05$ for values of the area above ξ^2 . b) Fractal dimension of the connected regions computed as the perimeter of each region versus their size, i.e. the square root of their area, yielding a value of $D = 7/4$.

III. CONCLUSIONS

To our knowledge, this is the first experimental measurement of the statistics of the velocity field in turbulent 2D quantum fluids. Our experiments show that the scale invariance of classical turbulence can be retrieved by considering velocity circulation instead of velocity increments. This suggests that circulation statistics is better suited for a universal description of quantum turbulence^{31,32}. Moreover, based on the scale-invariance of the circulations, we establish a connection with critical models in 2D. Real space analysis allows the identification of correlated vorticity regions with typical size ranging from ξ to 10ξ . We find that these regions share the same statistical behavior of critical percolation boundaries, enabling a series of predictions to be made on the properties of the inverse energy cascade in 2D quantum fluids. Optical systems provide a new experimental platform that can help unify the microscopic nature of vortex interactions with the large-scale symmetries of turbulent fluids³⁷⁻⁴⁵.

ACKNOWLEDGMENTS

The authors thank Guido Boffetta for useful discussions. The authors acknowledge the following projects: Italian Ministry of University (MUR) PRIN project “Interacting Photons in Polariton Circuits” – INPhoPOL (grant 2017P9FJBS); the project “Hardware implementation of a polariton neural network for neuromorphic computing” – Joint Bilateral Agreement CNR-RFBR (Russian Foundation for Basic Research) – Triennial Program 2021–2023; the MAECI project “Novel photonic platform for neuromorphic computing”, Joint Bilateral Project Italia-Polonia 2022-2023; PNRR MUR project “National Quantum Science and Technology Institute” - NQSTI (PE0000023); PNRR MUR project “Integrated Infrastructure Initiative in Photonic and Quantum Sciences” - I-PHOQS (IR0000016); Apulia Region, project “Progetto Tecnopolo per la Medicina di precisione”, Tecnomed 2 (grant number: Deliberazione della Giunta Regionale n. 2117 del 21/11/2018). The authors are grateful to P. Cazzato for the valuable technical support during the experiments.

Appendix A: Methods

To build a statistics for the connected regions of vorticity flux like the one shown in Fig. 3, we first compute the curl of the incompressible velocity field $\nabla \times \mathbf{u}(\mathbf{x})$ and then we construct the scalar field $\Gamma_R(\mathbf{x})$, for each image and for $R = [1.4\xi, 1.96\xi, 2.5\xi]$. The highest positive (minimum negative) value for this ensemble of fields $\Gamma_R(\mathbf{x})$ is what we use to set a threshold that is 5%, 10%, or 20% of this value. For each field every positive (negative) value that is greater (smaller) than said threshold is set to 1 (-1) while the rest is set to 0, resulting in the “binarized” images like the one in Fig. 3a.

To analyse the resulting connected regions we labelled them with the python `skimage.measure.label` module, using a 2-connectivity. The area of each region is the number of pixels of the region scaled by the pixel area, while the perimeter is approximated with a line through the centers of border pixels using a 4-connectivity.

- ¹U. Frisch, *Turbulence: The Legacy of A. N. Kolmogorov* (Cambridge University Press, 1995).
- ²R. Fjortoft, *Tellus* **5**, 225 (1953).
- ³R. H. Kraichnan, *The Physics of Fluids* **10**, 1417 (1967).
- ⁴G. Boffetta and R. E. Ecke, *Annual Review of Fluid Mechanics* **44**, 427 (2012).
- ⁵A. Alexakis and L. Biferale, *Phys. Rep.* **767**, 1 (2018).
- ⁶P. K. Yeung, X. M. Zhai, and K. R. Sreenivasan, *PNAS* **112**, 12633 (2015).
- ⁷R. Benzi, G. Paladin, G. Parisi, and A. Vulpiani, *Journal of Physics A: Mathematical and General* **17**, 3521 (1984).
- ⁸J. Paret and P. Tabeling, *Phys. Fluids* **10**, 3126–36 (1998).
- ⁹G. Boffetta, A. Celani, and M. Vergassola, *Phys. rev. E* **61**, R29 (2000).
- ¹⁰L. Onsager, *Il Nuovo Cimento* (1943-1954) **6**, 279 (1949).
- ¹¹G. L. Eyink and K. R. Sreenivasan, *Rev. Modern Phys.* **78**, 87 (2006).
- ¹²H. E. Hall, W. F. Vinen, and D. Shoenberg, *Proceedings of the Royal Society of London. Series A. Mathematical and Physical Sciences* **238**, 215 (1956).
- ¹³C. F. Barenghi, L. Skrbek, and K. R. Sreenivasan, *Proceedings of the National Academy of Sciences* **111**, 4647 (2014).
- ¹⁴E. A. L. Henn, J. A. Seman, G. Roati, K. M. F. Magalhães, and V. S. Bagnato, *Phys. Rev. Lett.* **103**, 045301 (2009).

- ¹⁵A. C. White, B. P. Anderson, and V. S. Bagnato, *Proceedings of the National Academy of Sciences* **111**, 4719 (2014).
- ¹⁶N. Navon, A. L. Gaunt, R. P. Smith, and Z. Hadzibabic, *Nature* **539**, 72 (2016).
- ¹⁷N. Navon, R. P. Smith, and Z. Hadzibabic, *Nature Physics* **17**, 1334 (2021).
- ¹⁸W. J. Kwon, G. Del Pace, K. Xhani, L. Galantucci, A. Muzi Falconi, M. Inguscio, F. Scazza, and G. Roati, *Nature* **600**, 64 (2021).
- ¹⁹S. P. Johnstone, A. J. Groszek, P. T. Starkey, C. J. Billington, T. P. Simula, and K. Helmerson, *Science* **364**, 1267 (2019).
- ²⁰G. Gauthier, M. T. Reeves, X. Yu, A. S. Bradley, M. A. Baker, T. A. Bell, H. Rubinsztein-Dunlop, M. J. Davis, and T. W. Neely, *Science* **364**, 1264 (2019).
- ²¹A. Skaugen and L. Angheluta, *Phys. Rev. E* **95**, 052144 (2017).
- ²²I. Carusotto and C. Ciuti, *Reviews of Modern Physics* **85**, 299 (2013).
- ²³A. Amo, D. Sanvitto, F. Laussy, D. Ballarini, E. d. Valle, M. Martin, A. Lemaître, J. Bloch, D. Krizhanovskii, M. Skolnick, *et al.*, *Nature* **457**, 291 (2009).
- ²⁴D. Caputo, D. Ballarini, G. Dagvadorj, C. Sánchez-Muñoz, M. DeGiorgi, L. Dominici, K. West, L. N. Pfeiffer, G. Gigli, F. P. Laussy, M. H. Szymańska, and D. Sanvitto, *Nat. Mater.* **17**, 145 (2018).
- ²⁵D. Ballarini, D. Caputo, G. Dagvadorj, R. Juggins, M. D. Giorgi, L. Dominici, K. West, L. N. Pfeiffer, G. Gigli, M. H. Szymańska, *et al.*, *Nature communications* **11**, 217 (2020).
- ²⁶R. Panico, P. Comaron, M. Matuszewski, A. S. Lanotte, D. Trypogeorgos, G. Gigli, M. D. Giorgi, V. Ardizzone, D. Sanvitto, and D. Ballarini, *Nature Photonics* **17**, 451 (2023).
- ²⁷S. Donati, L. Dominici, G. Dagvadorj, D. Ballarini, M. De Giorgi, A. Bramati, G. Gigli, Y. G. Rubo, M. H. Szymańska, and D. Sanvitto, *Proceedings of the National Academy of Sciences* **113**, 14926 (2016).
- ²⁸R. Panico, G. Macorini, L. Dominici, A. Gianfrate, A. Fieramosca, M. De Giorgi, G. Gigli, D. Sanvitto, A. S. Lanotte, and D. Ballarini, *Physical Review Letters* **127**, 047401 (2021).
- ²⁹I. Min, I. Mezić, and A. Leonard, *Physics of Fluids* **8**, 1169 (1996).
- ³⁰G. Sofiadis, I. E. Sarris, and A. Alexakis, *Physical Review Fluids* **8**, 024607 (2023).
- ³¹K. P. Iyer, K. R. Sreenivasan, and P. K. Yeung, *Phys. Rev. X* **9**, 041006 (2019).
- ³²J. I. Polanco, N. P. Mueller, and G. Krstulovic, *Nature Communications* **12**, 7090 (2021).
- ³³H.-Y. Zhu, J.-H. Xie, K.-Q. Xia, *et al.*, *Physical Review Letters* **130**, 214001 (2023).
- ³⁴D. Bernard, G. Boffetta, A. Celani, and G. Falkovich, *Nature Physics* **2**, 124 (2006).
- ³⁵L. Puggioni, A. G. Kritsuk, S. Musacchio, and G. Boffetta, *Physical Review E* **102**, 023107 (2020).
- ³⁶D. Stauffer and A. Aharony, *Introduction to percolation Theory* (Taylor & Francis, 2003).
- ³⁷D. Caputo, N. Bobrovska, D. Ballarini, M. Matuszewski, M. De Giorgi, L. Dominici, K. West, L. N. Pfeiffer, G. Gigli, and D. Sanvitto, *Nature Photonics* **13**, 488 (2019).
- ³⁸I. Liberal, M. Lobet, Y. Li, and N. Engheta, *Proceedings of the National Academy of Sciences* **117**, 24050 (2020).
- ³⁹A. A. Maître, F. Claude, G. Lerario, S. Koniakhin, S. Pigeon, D. Solnyshkov, G. Malpuech, Q. Glorieux, E. Giacobino, and A. Bramati, *Europhysics Letters* **134**, 24004 (2021).
- ⁴⁰A. Eloy, O. Boughdad, M. Albert, P. Larré, L. Mortessagne, M. Bellec, and C. Michel, *Europhysics Letters* **134**, 26001 (2021).
- ⁴¹T. Ferreira, V. Rocha, D. Silva, A. Guerreiro, and N. Silva, *New Journal of Physics* **24**, 113050 (2022).
- ⁴²H. Li, Z. Zhou, W. Sun, M. Lobet, N. Engheta, I. Liberal, and Y. Li, *Nature Communications* **13**, 4747 (2022).
- ⁴³M. Abobaker, W. Liu, T. Aladjidi, A. Bramati, and Q. Glorieux, *arXiv:2211.08441* (2023).
- ⁴⁴X. Bai, W. Wang, J. Zhang, Y. Wang, and Y. Xiang, *arXiv:2305.11884v2* (2023).
- ⁴⁵Y. Xiong, J. Chen, and X. Yu, *Communications in Theoretical Physics*, DOI 10.1088/1572 (2023).

Supplementary information for: Conformal-invariance of 2D quantum turbulence in an exciton-polariton fluid of light

R. Panico,¹ A. S. Lanotte,^{1,2} D. Trypogeorgos,¹ G. Gigli,^{1,3} M. De Giorgi,¹ D. Sanvitto,¹ and D. Ballarini¹

¹CNR NANOTEC, Institute of Nanotechnology, Via Monteroni, 73100 Lecce, Italy

²INFN, Sez. Lecce, 73100 Lecce, Italy

³Dipartimento di Matematica e Fisica E. De Giorgi, Università del Salento, Campus Ecotekne, via Monteroni, Lecce 73100, Italy

(*Electronic mail: dario.ballarini@nanotec.cnr.it)

(Dated: 3 July 2023)

I. COMPRESSIBILITY

All the observables presented in the main discussion are derived from the incompressible part of the density weighted velocity field $\mathbf{u}(\mathbf{x}, t) = \sqrt{\rho}(\mathbf{x}, t)\mathbf{v}(\mathbf{x}, t)$ where $\rho(\mathbf{x}, t)$ is the polariton fluid density and $\mathbf{v}(\mathbf{x}, t) = \frac{\hbar}{m}\nabla\theta(\mathbf{x}, t)$ its velocity (see Methods of Panico et al.¹). The superfluid itself however is also made of a compressible component and both contribute to the dynamics. We can quantify the degree of compressibility of our fluid using the standard definition $\mathcal{P} \equiv \mathcal{C}^2/\mathcal{S}^2$, where \mathcal{C} quantifies the compressible part with respect to the velocity gradient modulus, and $0 \leq \mathcal{P} \leq 1$ by definition,

$$\mathcal{P} = \frac{\langle (\partial_x u_x + \partial_y u_y)^2 \rangle}{\langle (\partial_x u_x)^2 + (\partial_y u_x)^2 + (\partial_x u_y)^2 + (\partial_y u_y)^2 \rangle}. \quad (\text{S1})$$

In our case, it yields $\mathcal{P} \simeq 0.43$.

II. SECOND ORDER MOMENT OF LONGITUDINAL VELOCITY INCREMENTS $\delta_r u$

To get further insight in the role of quantised vortices, we look at the scaling behaviour of the p-th order moments of the distributions of the velocity increments reported in the main text as a function of the scale r ,

$$S_p(r) = \left\langle \left| \frac{\mathbf{r}}{r} \cdot [\mathbf{u}(\mathbf{x} + \mathbf{r}) - \mathbf{u}(\mathbf{x})] \right|^p \right\rangle. \quad (\text{S2})$$

These exhibit a self-similar behaviour in the classical 2D inverse cascade, $S_p(r) \propto S_3^{p/3}(r) \sim r^{\frac{p}{3}2}$. Here we focus on the second-order moment $S_2(r)$ which is shown in Fig. S1, together with the fitted slope corresponding to the range $\xi < r < 2\xi$. Despite a small scaling region, it is possible to estimate the scaling exponent as 0.67 ± 0.02 , which corresponds to the Kolmogorov-like $-5/3$ scaling law of the energy spectrum in the inverse cascade according to the Wiener–Khinchin theorem. We note that turbulent scaling range is limited on the one hand by the presence on velocity jumps due to the quantised vortices, and on the other hand by the lack of stationarity at large scales.

III. NON TURBULENT CASE

We analyse the same system in the main text but for initial conditions that do not lead to a turbulent state¹. The statis-

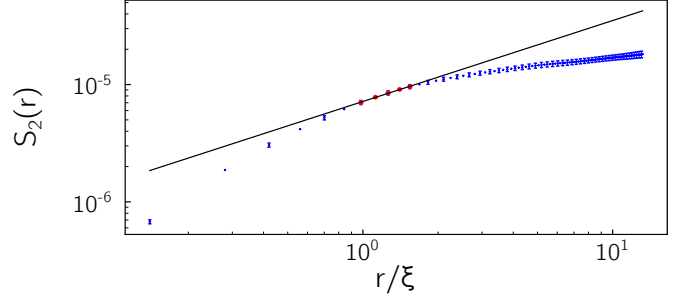


FIG. S1. Log-log plot of the second order moment of the incompressible velocity increments $\delta_r u \equiv \frac{\mathbf{r}}{r} \cdot [\mathbf{u}(\mathbf{x} + \mathbf{r}) - \mathbf{u}(\mathbf{x})]$ as a function of the scale. A scaling behaviour $S_2(r) \sim r^{\zeta_2}$ is expected within the turbulent scaling range: a slope is fitted in the scaling region of few healing lengths, which results in the value of the scaling exponent $\zeta_2 = 0.67 \pm 0.03$.

tics is constructed on a similar number of points. The normalised PDFs of the velocity increments in Fig. S2 are not self-similar, as expected given the quantised structure of the vortices, and exhibit a vortex-dominated behaviour as in the turbulent case illustrated in the main text. When the dimensionality of the system is measured using the same methods discussed in the main book, a noticeable difference emerges. In Fig. S3a, we report the number of connected regions of $\Gamma(\mathbf{x})$ with a given area $n(A)$, demonstrating how the points are much more spread and the scaling - if present - is slower than $\alpha = 96/91 + 1$. This indicates that the system has a lower tendency to arrange its structures over larger spatial scales. This is again confirmed by the fractal dimension measured as the perimeter $\mathcal{P}(A)$ versus the square root of the area A of the connected regions, as shown in Fig. S3b. In this case, for values above ξ , we can observe a scaling slightly lower than the one reported in Fig. 4b of the main text. It is also worth noting that ξ in this case differs from the one mentioned in the main text, and is of the order of $\xi \simeq 5.3 \mu\text{m}$. While the connected regions that form are clearly smaller and more scattered than in the turbulent case, the system begins to exhibit similar behaviour, and given enough time (limited by the polariton lifetime), it would most likely reach a very similar distribution of connected regions.

¹R. Panico, P. Comaron, M. Matuszewski, A. Lanotte, D. Trypogeorgos, G. Gigli, M. D. Giorgi, V. Ardizzone, D. Sanvitto, and D. Ballarini, Nature Photonics, 1 (2023).

²G. Boffetta, A. Celani, and M. Vergassola, Phys. rev. E **61**, R29 (2000).

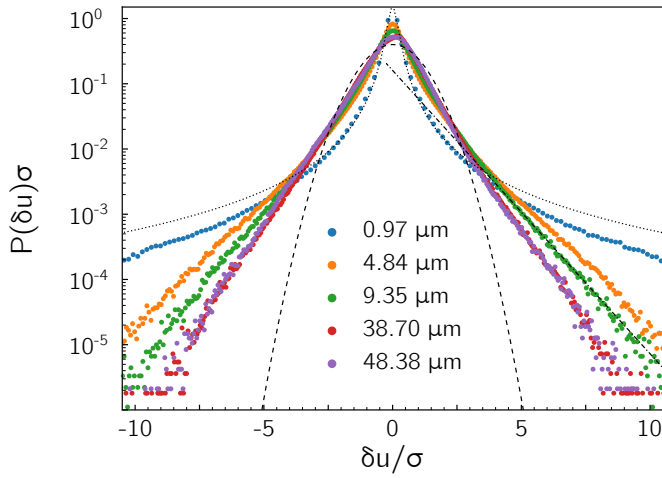


FIG. S2. a) Pdfs of the velocity increments $\frac{\mathbf{r}}{r} \cdot [\mathbf{u}(\mathbf{x} + \mathbf{r}) - \mathbf{u}(\mathbf{x})]$ for different \mathbf{r} , normalised with their respective standard deviation σ . As for the turbulent case for sub-healing length scales the pdf follows a Cauchy-Lorentz distribution (dotted line), while increasing \mathbf{r} it slowly approaches a Gaussian (dashed line).

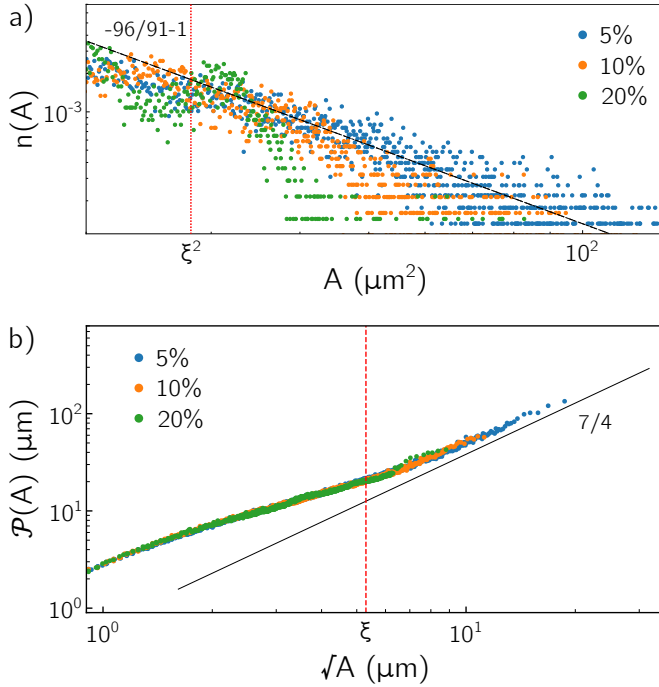


FIG. S3. a) Distribution of the extension of the connected area identified by thresholding the circulation. For the non turbulent case the points do not follow a well defined scaling. b) Fractal dimension of the connected regions computed as the perimeter of each region versus their size. The solid black line represent the $7/4$ scaling expected for a critical percolation, the dashed line indicates the actual scaling of the non turbulent case.

³L. Puggioni, A. G. Kritsuk, S. Musacchio, and G. Boffetta, Physical Review E **102**, 023107 (2020).